Journal of Power Sources 222 (2013) 52–58

Contents lists available at SciVerse ScienceDirect

Journal of Power Sources

journal homepage: www.elsevier.com/locate/jpowsour

High performance supercapacitor electrode based on graphene paper via flame-induced reduction of graphene oxide paper

Dongfei Sun [a,b,c], Xingbin Yan [a,b,*], Junwei Lang [a,b], Qunji Xue [b]

[a] Laboratory of Clean Energy Chemistry and Materials, Lanzhou Institute of Chemical Physics, Chinese Academy of Science, Lanzhou 730000, China
[b] State Key Laboratory of Solid Lubrication, Lanzhou Institute of Chemical Physics, Chinese Academy of Sciences, Lanzhou 730000, China
[c] Graduate University of Chinese Academy of Sciences, Beijing 100080, China

HIGHLIGHTS

- Reduced graphene oxide paper was prepared by direct flame reduction method.
- As-prepared graphene has high surface area and abundant oxygen containing groups.
- As-prepared graphene exhibited excellent supercapacitive performance.

GRAPHICAL ABSTRACT

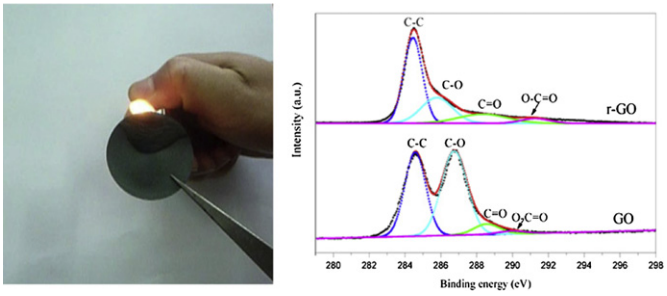

ARTICLE INFO

Article history:
Received 2 January 2012
Received in revised form
18 August 2012
Accepted 21 August 2012
Available online 1 September 2012

Keywords:
Flame-induced reduction
Graphene
Supercapacitor
Organic electrolyte

ABSTRACT

Reduced graphene oxide (r-GO) paper is easily synthesized by a flame-induced reduction of graphene oxide (GO) paper under ambient conditions. The X-ray diffraction and X-ray photoelectron spectroscope results confirm the effectivity of the flame-induced reduction. The resulting r-GO paper has a high surface area of 274.9 $m^2\ g^{-1}$ and contains a certain amount of oxygen-containing groups. Electrochemical behaviors of the electrode built with the r-GO paper are investigated in two kinds of electrolytes, 2 M KOH aqueous solution and 1 M Et_4NBF_4-acetonitrile solution, respectively. The results show that the high values of the specific capacitance for the r-GO can be obtained in both electrolytes, which reach 212 and 160 F g^{-1} at the same current density of 1 A g^{-1} respectively. Also, the r-GO-based electrode and supercapacitor exhibits stable cycling performance. The good capacitive performances in KOH aqueous electrolyte are due to the high surface area and the remaining oxygen containing groups of the r-GO paper.

1. Introduction

Graphene, a single layer of two-dimensional nanostructure sp^2 carbon material, owing to its high aspect ratio, excellent electrical conductivity, and good mechanical properties [1,2], has attracted great research in various applications, such as energy storage (including supercapacitors and various batteries) [3,4], polymer composites [5], nanoelectronics [6], sensors [7] and so on. Among these applications, graphene materials for supercapacitors seem to be extremely attractive for the present. Stoller et al. fabricated a symmetric supercapacitor based on chemically reduced graphene oxide (GO) to give a specific capacitance of 135 F g^{-1} in KOH and 99 F g^{-1} in an organic electrolyte [8]. Le et al. fabricated a supercapacitor using thermal-reduced GO, which has a specific

* Corresponding author. Laboratory of Clean Energy Chemistry and Materials, Lanzhou Institute of Chemical Physics, Chinese Academy of Science, Lanzhou 730000, China. Tel./fax: +86 931 4968055.
E-mail address: xbyan@licp.cas.cn (X. Yan).

0378-7753/$ – see front matter © 2012 Elsevier B.V. All rights reserved.
http://dx.doi.org/10.1016/j.jpowsour.2012.08.059

capacitance of 132 F g^{-1} in 1 M H_2SO_4 electrolyte [9]. And an electrochemically-reduced GO film has a specific capacitance of 128 F g^{-1} in 1 M $NaNO_3$ [10]. Meanwhile, different graphene-based materials were also prepared for supercapacitors [11–16].

To achieve the practical applications, many methods have been made to prepare graphene, mainly including micromechanical cleavage of highly oriented pyrolytic graphite (HOPG) [17], chemical exfoliation [18], chemical vapor deposition (CVD) [19,20], and arc discharge method [21]. Among them, the liquid-phase exfoliation method is considered to be the most effective way for large-scale and low-cost preparation of GO from graphite, and as-prepared GO can be converted to graphene by involving chemical reduction of GO using hydrazine or other reductants [22–24]. On the other hand, since the formation of GO paper by filtration was reported [25], this technique has been adopted for preparing graphene paper [26]. So the conversion from GO paper to graphene paper (the reduction/or deoxygenation process) has been realized by various methods, including chemical reduction [27], electrochemical reduction [10], thermal reduction [28], ion implantation [29], and flash-light induced reduction [30]. More recently, a hot soldering iron-assisted reduction method was reported by Kim et al. [31], which manifest a good reduction effect based on thermal reduction, just as the camera flashes [30]. And the r-GO paper can not to be burnt by post-flame treatment, indicating the good thermal stability of graphene against flame. As shown in the above methods [27–31], it is noteworthy that a temperature-depend condition is contributed to reduce GO. As we know, a transient high temperature would be provided by a flame. Therefore, it is expected that a suitable flame treatment on GO might be able to reduce GO and obtain graphene. However, the report on the reduction of GO based on a flame treatment is rare.

In this work, we report the preparation of r-GO paper by a rapid and clean flame-induced reduction of GO paper using a common lighter. Compared to other reduction methods, the advantages of our strategy is that this reduction process is very fast, easy operation, low cost, and without need of any reductant. Furthermore, this flame-induced reduction not only increases remarkably the surface area of the r-GO paper, but also retains appropriate content of oxygen containing groups on the graphene sheets. Therefore, the resulting r-GO paper exhibits excellent electrochemical capacitive properties in aqueous and organic electrolytes.

2. Experimental

2.1. Preparation of GO aqueous colloid and GO paper

GO was prepared by the modification of Hummers' method and described elsewhere [32,33]. The detailed synthesis process can also be found in our previous report [34]. 100 mg of GO solid was dispersed in 200 mL of H_2O (twice-distilled water with a resistance about 18 MΩ was used) with the aid of ultrasonication using a high power (600 W) ultrasonic pole for 1 h, followed by centrifugation at 3000 rpm for 15 min to remove a small quantity of precipitation, forming a black-brown GO aqueous colloid. This homogeneous dispersion was tested to be stable for several months. Twenty milliliters of the above colloid was diluted with 20 mL of H_2O and GO paper was prepared by filtration of the diluted dispersion through a Millipore filter (50 mm in diameter and 0.45 μm in pore size), followed by washing, air drying, and peeling off from the filter.

2.2. Preparation of r-GO paper

A dried GO paper was reduced by a flame using a commercial lighter (the type of lighter was intentionally chosen for its simplicity, the lighter was purchased from Xinhai lighter Co., Ltd.), and the main component of the combustion liquid is butane. The specific procedure is followed: the GO paper was stabled by a tweezers, and a commercial lighter was set aside, and the epitaxial flame was used to deal GO, 5 s later, the GO was reduced to r-GO. An intuition video can be seen from Video 1 (in Supporting information).

Supplementary video related to this article can be found at http://dx.doi.org/10.1016/j.jpowsour.2012.08.059.

2.3. Characterizations of GO paper and r-GO paper

The morphology and microstructure of the as-prepared GO and r-GO films were investigated using a FE-SEM (JSM-6701F). Chemical compositions and crystallite structures of the samples were determined by XRD (X′ Pert Pro, Philips) using Cu Kα radiation from 5° to 80° angles. The surface chemical species of the as-prepared GO and r-GO paper were examined on a Perkin–Elmer PHI-5702 multifunctional X-ray photoelectron spectroscope (XPS, Physical Electronics, USA) using Al Ka radiation of 1486.6 eV as the excitation source. Nitrogen adsorption–desorption isotherm measurements were performed on a Micromeritics ASAP 2020 volumetric adsorption analyzer at 77 K. Before adsorption–desorption isotherm measurements, the samples were outgassed at 80 °C for 10 h in the degas port of the analyzer. The Brunauer–Emmett–Teller (BET) method was utilized to calculate the specific surface area of each sample.

2.4. Electrode preparation and electrochemical measurements

The electrochemical properties of GO paper and r-GO paper were investigated using a CHI660D Electrochemical Working Station (Shanghai Chenhua, China). For preparing the working electrode (WE), 80 wt.% of r-GO (8 mg), 7.5 wt.% of acetylene black (>99.9%), 7.5 wt.% of graphite powder and 5.0 wt.% of poly (tetrafluoroethylene) were mixed together in an agate mortar until a homogeneous black powder was obtained. The resulting mixture was pressed onto a foam nickel plate (as electric connection) at 10 MPa. The assembled electrode was dried at 60 °C for 16 h in air. All electrochemical measurements were carried out in a conventional glass electrochemistry cell with a three-electrode system in 2 M KOH aqueous solution and 1 M Et_4NBF_4 in acetonitrile at RT: a WE, a platinum wire counter electrode and a saturated calomel electrode (SCE) reference electrode. The cyclic voltammetry (CV) measurements were conducted at different scan rates ranging from 10 to 200 mV s^{-1} with a potential window from −1 V to 0 V in 2 M KOH and from −1.5 to 1.1 V in Et_4NBF_4 electrolyte, respectively. Galvanostatic charge/discharge measurements were run on from −1 to 0 V (in 2 M KOH electrolyte) and from −1.5 to 1.1 V (in Et_4NBF_4 electrolyte) at different current densities, and at open circuit potential. The C was calculated from the slope of each discharge curve, according to the equation $C = (I \times \Delta t)/(\Delta V \times m)$ [35], where C is the specific capacitance, I is the constant discharge current, Δt is the discharge time, ΔV is the voltage difference in discharge and m is the mass of r-GO coated on each WE. Electrochemical impedance spectroscopy (EIS) measurement was recorded from 10 kHz to 100 mHz with an alternate current amplitude of 5 mV. The cycling stability test was evaluated with a Land CT2001A battery program-control test system (LAND, Wuhan, China).

2.5. Electrochemical measurements in two-electrode system

Two symmetric capacitors (r-GO/r-GO supercapacitor and commercial activated carbon (AC, Kuraray, Japan, YP17, 1519 m^2 g^{-1})/AC supercapacitor) were fabricated for comparison. The electrodes

were prepared using nickel foam as the current collector; each electrode contained 4 mg of electrochemical active material and had a geometric surface area of about 1 cm^2. The cathode and anode electrode were pressed together and separated by a porous nonwoven cloth separator. The electrochemical measurements of the symmetric supercapacitors were carried out in 2 M KOH aqueous electrolyte using the electrochemical working station in a two-electrode cell at room temperature.

The specific capacitance, energy density and power density of the supercapacitors were estimated, using the following equations [15,35]:

$$C_m = I \times \Delta t / \Delta V \times m \quad (1)$$

$$C_{sp} = 4 \times C_m \quad (2)$$

$$E = 0.5\, C_m (\Delta V)^2 / 3.6 \quad (3)$$

$$P = E \times 3600 / \Delta t \quad (4)$$

Where C_m (F g^{-1}) is the measured device capacitance, I (A) represents constant discharging current, ΔV (V) refers to the potential window during the discharge process after IR drop, m (g) is the total mass of the active material on the two electrodes, C_{sp} is the specific capacitance of a single electrode in the two-electrode cell, E (W h kg^{-1}) refers to the energy density, P (kW kg^{-1}) corresponds to the power density.

3. Results and discussion

3.1. Morphology and chemical compositions of GO and r-GO

An intuition process can be seen from Video 1 (in Supporting Information). It is noteworthy that the reduction process was very rapid and the whole reduction just needed about 5 s once the flame was set on the side of the GO paper. We believe that the transient high temperature provided by the lighter flame triggered the reduction of the edge of the GO paper and the heat released from the initial GO reduction reaction was sufficient to trigger more completed reduction toward other directions of the GO paper. Moreover, good thermal conductivity for GO paper was another reason to achieve the rapid reduction process [36,37]. Fig. 1 shows the photographs and SEM images of GO and r-GO papers. The black GO and r-GO papers can be observed in Fig. 1a and b, respectively. After reduction, the r-GO paper still retains the structural integrity

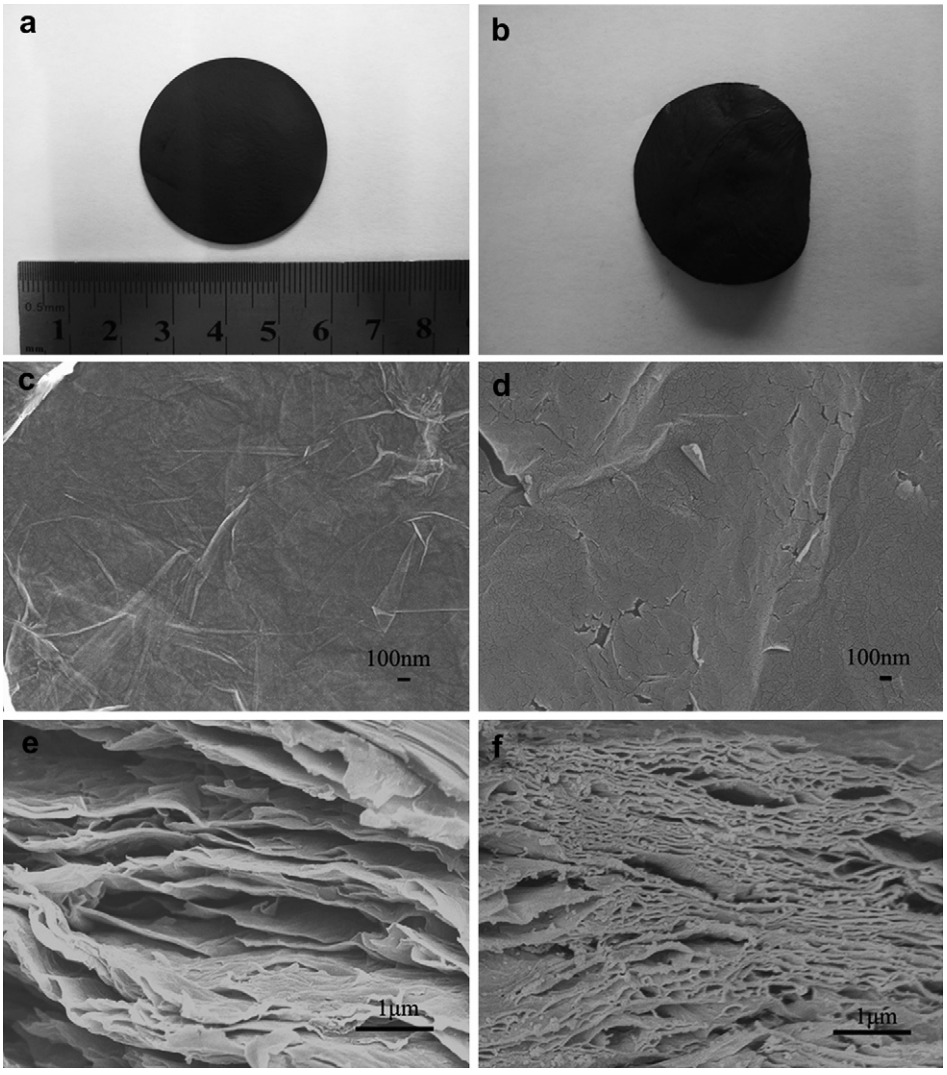

Fig. 1. Photographs of (a) GO and (b) r-GO papers, SEM images of (c and e) GO paper and (d and f) r-GO paper. c and d are top-view images, e and f are side-view images.

of the paper, which is in good agreement with the report on the flame retardancy of r-GO [31]. Compared with the GO paper, a rougher surface can be observed on the surface of r-GO, and the r-GO films typically expanded tens of times after flaming reduction. The thickness expansion of the flamed film suggested that the r-GO sheets were well exfoliated [30]. The morphology of the GO and r-GO was further investigated by SEM. Fig. 1c–f shows the surface and cross-sectional SEM images of the GO and r-GO paper. From the surface SEM images, a wrinkle-like morphology can be observed on the surface of GO, after reduction, a rougher surface and many apparent cracks can be observed on the surface of r-GO sheets. Fig. 1e and f shows the cross-sectional SEM images of the GO and r-GO paper, the fracture edges of the two samples all exhibit a layered structure. Moreover, the intact layered structure were seen after flame reduction, and the cross-sectional of r-GO is thicker and looser than GO paper, which induced by the high-temperature reduction process.

The XRD patterns of the GO and the r-GO samples are shown in Fig. 2a. In the XRD pattern of the GO, only one sharp peak around 2θ=9.7° can be detected, which corresponding to the (002) plane of graphene oxide. After reduction, the GO peak disappeared and a sharp peak at 23.1° emerged, it indicates that the high degree of the deoxygenation of the GO paper and the GO was reduced to graphene. This reduction result was also confirmed by the XPS pattern as the following. It is known that the performance of carbon materials as electrodes for supercapacitors is highly dependent on their specific surface area [38]. Fig. 2b shows the typical N_2 adsorption–desorption isotherm of GO and r-GO samples. The BET specific surface area of r-GO sample is 274.9 $m^2\ g^{-1}$, which is much higher than that of the GO sample (17.7 $m^2\ g^{-1}$), it indicates that the r-GO is further exfoliated, and the BET specific surface area of r-GO is also higher than the value of 106 $m^2\ g^{-1}$ for hydrazine reduced graphene reported by Wang et al. [39]. But the BET surface areas of r-GO sample are lower than the theoretical limit (2630 $m^2\ g^{-1}$) of graphene. It indicates that the r-GO is not completely exfoliated and some stacked graphitic layers are still existence in the sample [40,41].

XPS is an effective surface chemical analysis technique, which is used to determine the species and chemical states of the elements in the surface of the materials. To further explore the formation of r-GO, XPS was adopted for analyzing the composition of the GO and r-GO sheets. Fig. 3 shows the C1 XPS results for the GO and r-GO sheets. As shown in Fig. 3a, the XPS spectrum of C1s for GO can be divided in to four different peaks, which corresponded to the signal of C–C (at 284.6), C–O (at 286.7), C=O (at 288.6), and O–C=O (at 290.1) [22]. Among these, the C–C and C–O bonds dominated, indicating the considerable degree of oxidation in the GO paper.

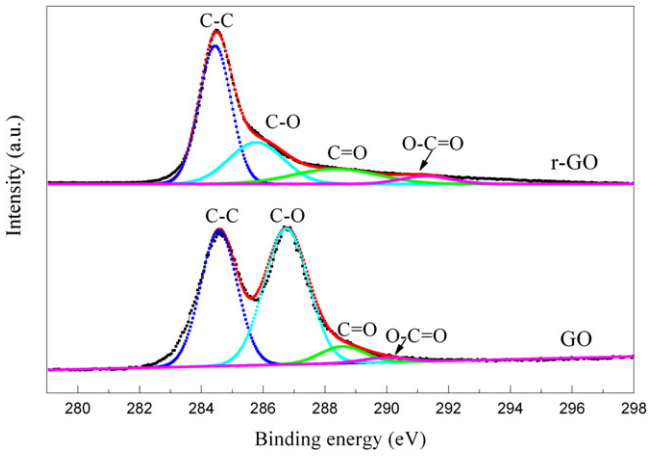

Fig. 3. The C 1s XPS spectra of GO and r-GO papers.

After reduction, the C1s XPS spectrum of r-GO paper also presented the same components by compared with the C1s XPS spectrum of GO paper, the intensity of the peak attributed to C–C bonds was dominant in the spectrum, and the peak intensities for C–O, C=O and O–C=O peaks are much smaller than those in GO paper, it is seen that the dominant C–O peak for GO (Fig. 3a) was dramatically decreased in the r-GO composite (Fig. 3b), indicating that high temperature facilitated the removal of hydroxyl groups, suggesting the efficient deoxygenation of GO and the formation of graphene that occurred via flame-treatment, and our results are in good agreement with the report by Cuong et al. [42]. In addition, it is need to emphasize that more oxygen composition was remained in r-GO, about 14% (atomic), it suggests that the prepared graphene with high oxygen ratio is obtained by the flame-induced reduction. And the oxygen remained in r-GO is higher than the produce by chemical reduction using hydrazine hydrate as reducing reagent [43]. The oxygen containing groups, such as pyrone-like functionalities (part of C=O and C–O) in the surface of carbon materials can make effects on the electrochemical behaviors [35]. Therefore, it can be inferred that higher oxygen composition is also beneficial for the r-GO in supercapacitors through pseudo-faradic reactions of these oxygen active groups [35,44].

3.2. Electrochemical performance of the capacitors

The electrochemical properties of the r-GO were studied by CV, galvanostatic charge–discharge and EIS in 2 M KOH aqueous

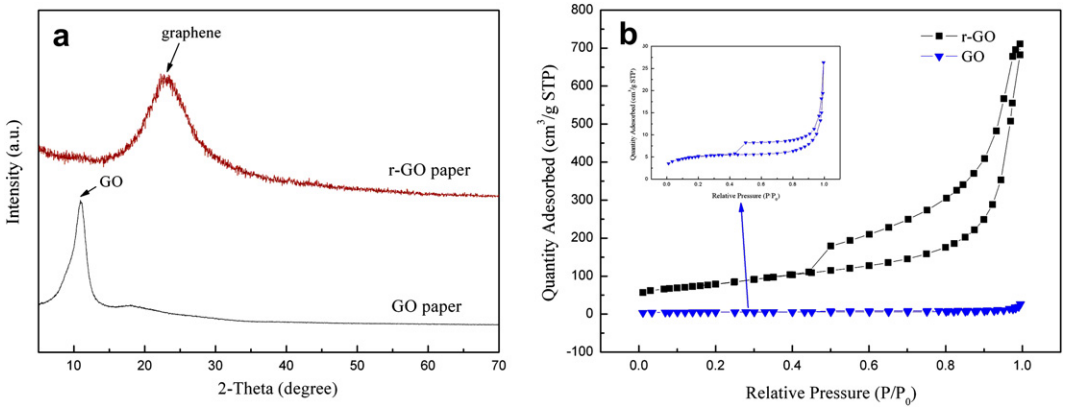

Fig. 2. (a) XRD patterns and (b) N_2 adsorption–desorption isotherms of GO and r-GO paper samples.

solution and 1 M Et_4NBF_4 in acetonitrile, respectively. From the CV curves of GO and r-GO electrodes in 2 M KOH aqueous solution (Fig. S1), it can be seen that the r-GO electrode has higher activity area than GO electrode (Fig. S1a), which can be further demonstrated by the galvanostatic charge–discharge result (Fig. S1b). Fig. 4a shows CV curves of r-GO sample with various scan rates in the range of −1 to 0 V in 2 M KOH aqueous solution, and r-GO electrode exhibited fairly rectangular CV curves which is indicative of double layer capacitor behavior. Also, the current density response gradually increased with the increase of the voltage sweep rate. To examine the electrochemical behavior of r-GO in organic electrolyte, CV tests were detected in 1 M Et_4NBF_4 in acetonitrile. And the CV tests were conducted within a range of −2.1–1.2 V (Fig. S2), it can be seen that r-GO electrode has higher potential Window (3.3 V), and a suitable potential Window of −1.5–1.1 V was chose to discuss the electrochemical properties. Fig. 4b shows CV curves of r-GO sample with various scan rates in the range of −1.5 to 1.1 V, we can found that the CV curves of r-GO in organic electrolyte also presents rectangular shape, which is also indicative of double layer capacitor behavior in organic electrolyte, it indicates that different kinds of electrolyte has a little affect on the electrochemical properties of r-GO.

Fig. 5 shows the galvanostatic charge–discharge curves of the r-GO at different current density in the range of 1.0–5.0 A g^{-1} in 2 M KOH aqueous solution (Fig. 5a) and 1 M Et_4NBF_4 in acetonitrile (Fig. 5c), respectively. It is clearly seen that all of the charging/discharging curves were fairly linear, again demonstrating capacitive behavior, and the specific capacitance gradually decreased with the increase of discharge current density. According to the capacitance equation evaluated from the slopes of the discharge curves (shown in the Experimental section), the specific capacitance of r-GO in different electrolyte obtained at different current densities (1.0, 2.0, 3.0, 4.0 and 5.0 A g^{-1}) was summarized in Fig. 5b and d, respectively. When the current density was increased from 1.0 to 5.0 A g^{-1}, the specific capacitance of the sample decreased from 212 to 160 F g^{-1} in 2 M KOH, and from 160 to 96 F g^{-1} in 1 M Et_4NBF_4 electrolyte. Fig. 5c and d further shows an obvious decrease of capacitance with current densities. The high capacitance of 212 and 160 F g^{-1} were obtained at 1 A g^{-1} by using 2 M KOH aqueous and 1 M Et_4NBF_4 as electrolyte, respectively. The high capacitance is greatly dependent on the high specific surface area. Specifically, after flame reduction, some oxygen containing groups was preserved, and the high oxygen composition is beneficial for supercapacitors in KOH aqueous electrolyte. Moreover, the thermal reduction play an important role in the flame reduction process, and the thermal decomposition process of the lactone–ether pairs leaves C vacancies saturated by ether groups [45], it is important to preserve a high oxygen composition in r-GO. And the residual oxygen containing groups on the surface of r-GO also greatly affects the electrochemical capacitance in supercapacitors.

EIS is used to investigate the performance of electrochemical capacitors such as internal resistance, capacity, etc [46]. The EIS data are analyzed using Nyquist plots, which show the frequency response of the electrode/electrolyte system and are the plots of the imaginary component (Z″) of the impedance against the real component (Z′). Fig. 6 shows the relation between Z″ and Z′ impedance components of r-GO in different electrolyte. The complex-plane impedance plot for r-GO sample could be divided into the high-frequency component and the low-frequency component. A distinct knee in the frequency was observed in the high-frequency component in the set of Fig. 6, respectively. The equivalent series resistance (ESR) of the r-GO electrode can be obtained from the *x* intercept of the Nyquist plot, the ESR of r-GO electrode were 0.93 and 2.63 Ω in KOH and Et_4NBF_4 electrolyte, respectively. The value includes the total combination of the ionic resistance of electrolyte, intrinsic resistance of active materials and contact resistance at the active material–current collector interface. Obviously, the intrinsic resistance for our r-GO electrode is low in our system, and the flame-treatment has a large contribution to the overall ESR. The impedance of the low-frequency region is attributed to the diffusion process of ions in the graphite layer [47]. Moreover, both of two spectra show a Warburg angle higher than 45° in the low frequencies, implying the electrode was strongly controlled by ion diffusion/transport process. All of the reasons indicated that the r-GO is suitable as the electrode materials for supercapacitors.

Cycle life is one of the most electrochemical performances of supercapacitors. The cyclability of r-GO electrodes were examined by galvanostatic charge-discharge measurement in both two electrolytes at a current density of 4 A g^{-1} (Fig. 7a and b). The r-GO electrode displayed excellent stability in potential window of 1.0 and 2.6 V, respectively. Fig. 7a illustrates the change in specific capacitance of the electrode recorded during 2000 cycles in 2 M KOH electrolyte, the specific capacitance showed slight decrease at the initial 500 cycles, and then remained stable with increasing cycles number and only about 16% specific capacitance was dropped after 2000 cycles. When the Et_4NBF_4 was used as electrolyte (Fig. 7b), the r-GO electrode also displayed excellent stability. However, the specific capacitance showed a great decrease at the initial 250 cycles, which may be resulted from the expansion of the electrode material and lead to bad contact between electrode material and current collector. Then remained stable with increasing cycle number, and about 59% specific capacitance was preserved 2000 cycles. The above results reveal that the r-GO sample shows excellent cycle stability in both electrolytes.

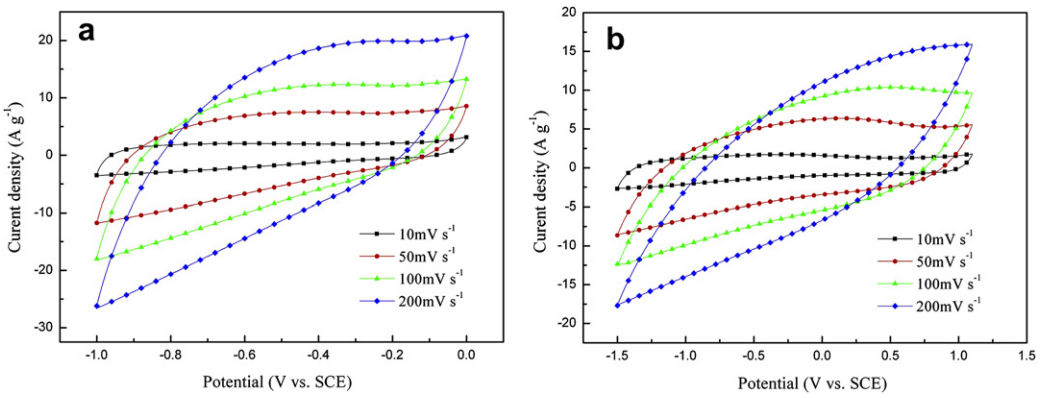

Fig. 4. CV curves of r-GO papers scanned at different rates in 2 M KOH (a) and 1 M Et_4NBF_4-acetonitrile electrolytes (b), respectively.

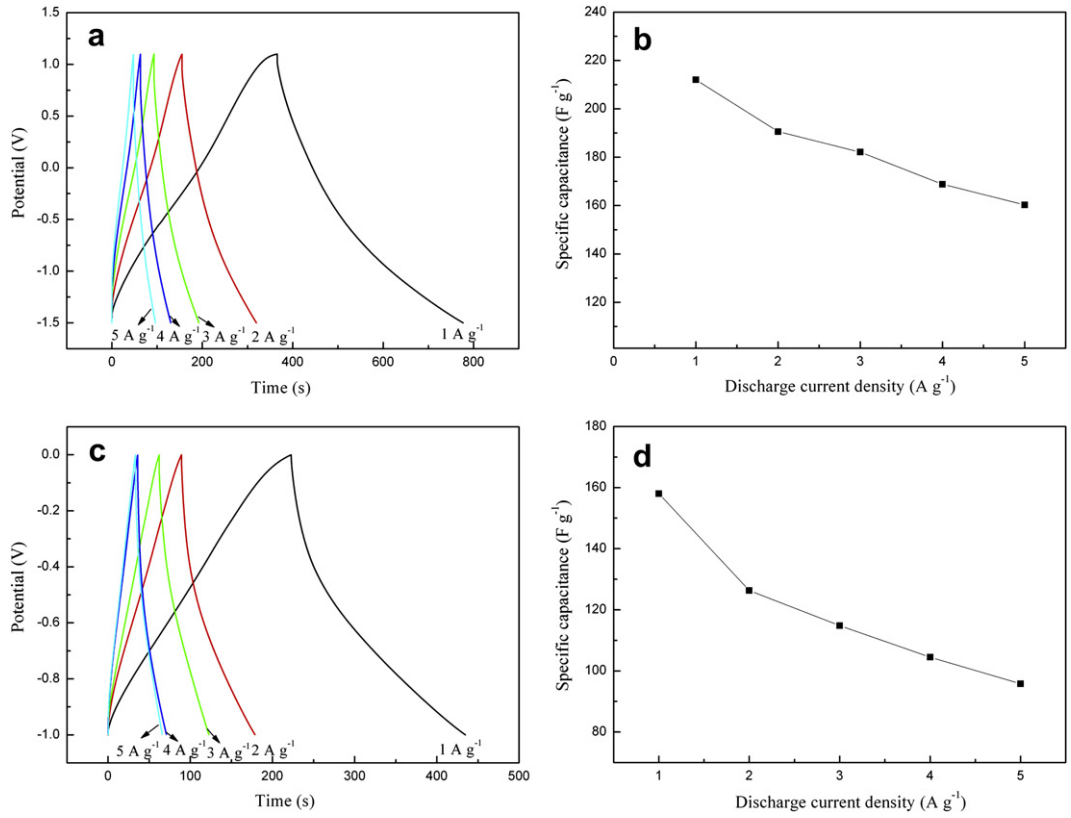

Fig. 5. Galvanostatic charge–discharge curves of r-GO at different current densities in 2 M KOH (a) and 1 M Et_4NBF_4-acetonitrile electrolytes (c). (b) and (d) The specific capacitance variation curves with current density, corresponding to (a) and (c), respectively.

3.3. Electrochemical performance in two-electrode system

To completely investigate the electrochemical performance of the r-GO sample, the r-GO/r-GO supercapacitor was estimated in 2 M KOH aqueous solution, for comparing, commercial AC/AC supercapacitor was also studied. The values of specific capacitance (the cell and the single electrode in the cell), energy density and power density are summarized in Table 1. The results show that the specific capacitance, energy density and power density of the r-GO-based supercapacitor are higher than those of the AC-based supercapacitor in KOH electrolyte. Therefore, the r-GO materials could be used for the preparation of carbon supercapacitors with KOH aqueous electrolyte. However, the specific capacitance of r-GO obtained from two-electrode system is lower than that obtained from three-electrode system. This phenomenon is very normal for electrode materials [48]. The cyclability of r-GO-based supercapacitor was examined by galvanostatic charge–discharge

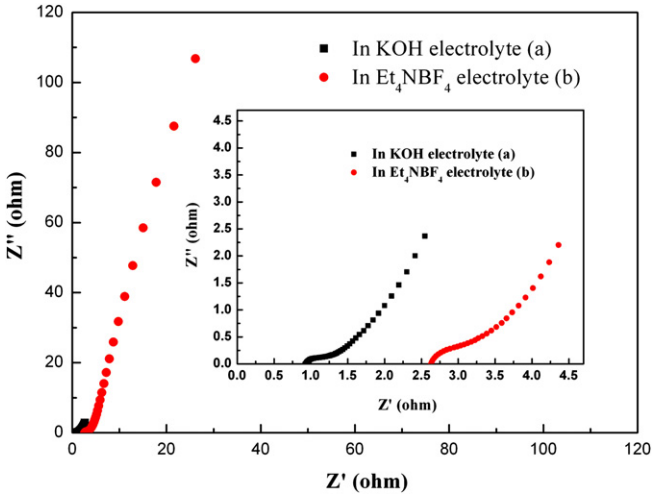

Fig. 6. Nyquist plot of r-GO obtained in 2 M KOH (a) and 1 M Et_4NBF_4-acetonitrile electrolytes (b). Inset is the enlarged plot of the high-frequency regions.

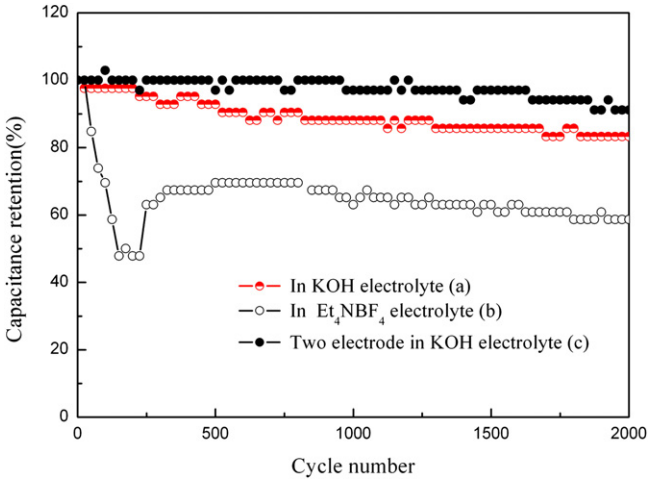

Fig. 7. The specific capacitance change of r-GO electrode at a current density of 4 A g^{-1} in 2 M KOH (a) and 1 M Et_4NBF_4-acetonitrile (b) electrolytes, respectively. A cyclability of r-GO-based supercapacitor was examined at a current density of 1 A g^{-1} in 2 M KOH aqueous electrolyte (c).

Table 1
Values of specific capacitance, energy density and power density depending on cell types.

Electrode material	KOH electrolyte				
	The specific capacitance of single electrode in three-electrode cell (F g^{-1})	Two-electrode cell			
		The specific capacitance of single electrode in two-electrode cell (F g^{-1})	The specific capacitance of the cell (F g^{-1})	Energy density (Wh kg^{-1}) and power density (W kg^{-1}) at the current density of 1 A g^{-1}	Energy density (Wh kg^{-1}) and power density (W kg^{-1}) at the current density of 10 A g^{-1}
r-GO	212	175	43.9	6.10/500.2	4.86/4998.9
AC	135	102	25.5	3.54/499.8	1.68/3571

measurement at a current density of 1 A g^{-1} in 2 M KOH aqueous electrolyte (Fig. 7c), the supercapacitor exhibits excellent cycle stability, and it can retain over 91% of its capacitance over 2000 cycles. These results demonstrate that the as-prepared r-GO paper is a potential candidate for supercapacitor materials with high capacity, good cycle performance and high degree of reversibility in the repetitive charge-discharge cycling.

4. Conclusions

A simple and effective flame-induced reduction has been employed to prepare r-GO paper under ambient conditions. The resulting r-GO paper has a high surface area of 274.9 m^2 g^{-1}. The r-GO paper exhibits excellent electrochemical properties and the specific capacitance reaches about 212 and 160 F g^{-1} in 2 M KOH aqueous solution and 1 M Et_4NBF_4–acetonitrile solution, respectively. Specially, the good supercapacitive performances in KOH aqueous solution are greatly benefited from the high surface area and the abundant oxygen containing groups. Also, the r-GO paper shows excellent cycle stability. Therefore, such flame-induced reduction could provide a highly efficient and environment friendly method to reduce GO for energy storage application.

Acknowledgments

This work was supported by the Top Hundred Talents Program of Chinese Academy of Sciences and the National Nature Science Foundation of China (51005225).

Appendix A. Supporting information

Supplementary data related to this article can be found at http://dx.doi.org/10.1016/j.jpowsour.2012.08.059.

References

[1] S. Stankovich, D.A. Dikin, G.H.B. Dommett, K.M. Kohlhaas, E.J. Zimney, E.A. Stach, R.D. Piner, S.T. Nguyen, R.S. Ruoff, Nature 442 (2006) 282–286.
[2] S. Guo, S. Dong, Chem. Soc. Rev. 40 (2011) 2644–2672.
[3] C. Wang, D. Li, C.O. Too, G.G. Wallace, Chem. Mater. 21 (2009) 2604–2606.
[4] Y. Wang, Z.Q. Shi, Y. Huang, Y.F. Ma, C.Y. Wang, M.M. Chen, Y.S. Chen, J. Phys. Chem. C 113 (2009) 13103–13107.
[5] J.L. Vickery, A.J. Patil, S. Mann, Adv. Mater. 21 (2009) 2180–2184.
[6] C. Berger, Z.M. Song, T.B. Li, X.B. Li, A.Y. Ogbazghi, R. Feng, Z.T. Dai, A.N. Marchenkov, E.H. Conrad, P.N. First, W.A.D. Heer, J. Phys. Chem. B 108 (2004) 19912–19916.
[7] C.H. Lu, H.H. Yang, C.L. Zhu, X. Chen, G.N. . Chen, Angew. Chem. Int. Ed. 48 (2009) 4785–4787.
[8] M.D. Stoller, S. Park, Y. Zhu, J. An, R.S. Ruoff, Nano. Lett. 8 (2008) 3498–3502.
[9] L.T. Le, M.H. Ervin, H. Qiu, B.E. Fuchs, W.Y. Lee, Electrochem. Commun. 13 (2011) 355–358.
[10] X.Y. Peng, X.X. Liu, D. Diamond, K.T. Lau, Carbon 49 (2011) 3488–3496.
[11] X.M. Feng, R.M. Li, Y.M. Ma, R.F. Chen, N.E. Shi, Q.L. Fan, W. Huang, Adv. Funct. Mater. 21 (2011) 2989–2996.
[12] J. Yoo, K. Balakrishnan, J. Huang, V. Meunier, B. Sumpter, A. Srivastava, M. Conway, A. Reddy, J. Yu, R. Vajtai, P. Ajayan, Nano. Lett. 11 (2010) 1423–1427.
[13] R.B. Rakhi, H.N. Alshareer, J. Power Sources 196 (2011) 8858–8865.
[14] J.T. Zhang, J.W. Jiang, H.L. Li, X.S. Zhao, Energy Environ. Sci. 4 (2011) 4009–4015.
[15] C.G. Liu, Z.N. Yu, D. Neff, A. Zhamu, B.Z. Jang, Nano. Lett. 10 (2010) 4863–4868.
[16] G.H. Yu, L.B. Hu, N.A. Liu, H.L. Wang, M. Vosgueritchian, Y. Yang, Y. Cui, Z.A. Bao, Nano Lett. 11 (2011) 4438–4442.
[17] S. Park, H.C. Floresca, Y. Suh, M.J. Kim, Carbon 48 (2010) 797–804.
[18] Y. Hernandez, V. Nicolosi, M. Lotya, F.M. Blighe, Z. Sun, S. De, I.T. McGovern, B. Holland, M. Byrne, Y.K. Gun'Ko, J.J. Boland, P. Niraj, G. Duesberg, S. Krishnamurthy, R. Goodhue, J. Hutchison, V. Scardaci, A.C. Ferrari, J.N. Coleman, Nat. Nanotechnol. 3 (2008) 563–568.
[19] Z.P. Chen, W.C. Ren, L.B. Gao, B.L. Liu, S.F. Pei, H.M. Cheng, Nat. Mater. 10 (2011) 424–428.
[20] X. Li, W. Cai, J. An, S. Kim, J. Nah, D. Yang, R. Piner, A. Velamakanni, I. Jung, E. Tutuc, S.K. Banerjee, L. Colombo, R.S. Ruoff, Science 324 (2009) 1312–1314.
[21] Y. Wu, B. Wang, Y. Ma, Y. Huang, N. Li, F. Zhang, Y. Chen, Nano. Res. 3 (2010) 661–669.
[22] S. Park, J. An, J.R. Potts, A. Velamakanni, S. Murali, R.S. Ruoff, Carbon 49 (2011) 3019–3023.
[23] S. Dubin, G. Scott, K. Wang, V.C. Tung, K. Cha, A.S. Hall, J. Farrar, R. Varshneya, Y. Yang, R.B. Kaner, ACS Nano 4 (2010) 3845–3856.
[24] W.F. Chen, L.F. Yan, P.R. Bangal, J. Phys. Chem. C 114 (2010) 19885–19890.
[25] D.A. Dikin, S. Stankovich, E.J. Zimney, R.D. Piner, G.H.B. Dommett, G. Evmenenko, S.T. Nguyen, R.S. Ruoff, Nature 448 (2007) 457–460.
[26] H. Chen, M.B. Müller, K.J. Gilmore, G.G. Wallace, D. Li, Adv. Mater. 20 (2008) 3557–3561.
[27] S.F. Pei, J.P. Zhao, J.H. Du, W.C. Ren, H.M. Cheng, Carbon 48 (2010) 4466–4474.
[28] J.L. Xiang, L.T. Drzal, Carbon 49 (2011) 773–778.
[29] J.T. Chen, G.A. Zhang, B.M. Luo, D.F. Sun, X.B. Yan, Q.J. Xue, Carbon 49 (2011) 3141–3147.
[30] L.J. Cote, R. Cruz-Silva, J.X. Huang, J. Am. Chem. Soc. 131 (2009) 11027–11032.
[31] F. Kim, J. Luo, R. Cruz-Silva, L.J. Cote, K. Sohn, J.X. Huang, Adv. Funct. Mater. 20 (2010) 2867–2873.
[32] Y.X. Xu, H. Bai, G.W. Lu, C. Li, G.Q. Shi, J. Am. Chem. Soc. 130 (2008) 5856–5857.
[33] W.S. Hummers Jr., R.E. Offeman, J. Am. Chem. Soc. 80 (1958). 1339–1339.
[34] X.B. Yan, J.T. Chen, J. Yang, Q.J. Xue, P. Miele, ACS Appl. Mater. Interfaces 2 (2010) 2521–2529.
[35] J.W. Lang, X.B. Yan, X.Y. Yuan, J. Yang, Q.J. Xue, J. Power Sources 196 (2011) 10472–10478.
[36] A.A. Balandin, Nat. Mater. 10 (2011) 569–581.
[37] S.R. Wang, M. Tambraparni, J.J. Qiu, J. Tipton, D. Dean, Macromolecules 42 (2009) 5251–5255.
[38] E. Frackowiak, F. Béguin, Carbon 39 (2001) 937–950.
[39] D.W. Wang, F. Li, Z.S. Wu, W.C. Ren, H.M. Cheng, Electrochem. Commun. 11 (2009) 1729–1732.
[40] M.J. McAllister, J.L. Li, D.H. Adamson, H.C. Schniepp, A.A. Abdala, J. Liu, H.A. Margarita, D.L. Milius, R. Car, R.K. Prud'homme, I.A. Aksay, Chem. Mater. 19 (2007) 4396–4404.
[41] Q.L. Du, M.B. Zheng, L.F. Zhang, Y.W. Wang, J.H. Chen, L.P. Xue, W.J. Dai, G.B. Ji, J.M. Cao, Electrochim. Acta 55 (2010) 3897–3903.
[42] T.V. Cuong, V.H. Pham, E.W. Shin, J.S. Chung, S.H. Hur, E.J. Kim, Q.T. Tran, H.H. Nguyen, P.A. Kohl, Appl. Phys. Lett. 99 (2011) 041905–041908.
[43] P.G. Ren, D.X. Yan, X. Ji, T. Chen, Z.M. Li, Nanotechnology 22 (2011) 055705–055713.
[44] V. Khomenko, E. Raymundo-Piñero, F. Béguin, J. Power Sources 195 (2010) 4234–4241.
[45] R. Larciprete, S. Fabris, T. Sun, P. Lacovig, A. Baraldi, S. Lizzit, J. Am. Chem. Soc. 133 (2011) 17315–17321.
[46] G.H. Sun, K.X. Li, C.G. Sun, Micropor. Mesopor. Mater. 128 (2010) 56–61.
[47] C.T. Hsieh, S.M. Hsu, J.Y. Lin, H.S. Teng, J. Phys. Chem. C 115 (2011) 12367–12374.
[48] M.D. Stoller, R.S. Ruoff, Energy Environ. Sci. 3 (2010) 1294–1301.